Journal of Computer Science and Artificial Intelligence
ISSN: 3078-8242 (Print), ISSN: 3078-2309 (Online) | Vol. 5, No. 2, 2025

Hierarchical Measurement Model of Semiconductor Silicon Carbide Epilayer Thickness Based on Infrared Interferometry

Bowen Ye

College of International Education, Shenyang University, Shenyang, China
371271516@qq.com

Abstract: This paper proposes a hierarchical measurement model for silicon carbide (SiC) epilayer thickness based on infrared interferometry. Under a dual-beam interference framework, an analytical relationship between thickness and fringe spacing is established by integrating the Sellmeier dispersion model, resolving systematic errors caused by the constant refractive index assumption. For measured spectra, a five-step inversion algorithm is designed: Savitzky-Golay filtering suppresses noise, while robust spacing statistics combined with significant peak identification enable high-precision SiC thickness inversion at 10° and 15° incidence angles. Furthermore, four necessary conditions for multi-beam interference are derived, confirming significant Fabry-Pérot effects in silicon samples (Attachments 3–4). An Airy-function-based full-spectrum nonlinear fitting correction strategy is proposed, compressing systematic deviations from 5.2% to 1.5%. Experiments show: SiC measurements exhibit a coefficient of variation (CV) of 6.1% with multi-angle consistency $\delta < 10\%$; corrected silicon thickness is 6.6 μm; interference fringe spacing inversely correlates with thickness.

Keywords: Hierarchical Measurement Model, Epilayer Thickness, Infrared Interferometry, Five-step inversion algorithm, Airy-function.

1. Introduction

Silicon carbide, as a core third-generation semiconductor material, has its epilayer thickness directly influencing the breakdown voltage and conduction characteristics of power devices.

Traditional dual-beam models introduce significant systematic errors in broadband measurements by ignoring material dispersion. Recent studies improve accuracy by incorporating dispersion correction models. Zhang et al. [1] integrated the Sellmeier dispersion equation into dual-beam optical path difference calculations, reducing angle-dependent deviation in SiC thickness measurements to below 3%. For oblique-incidence geometric correction, Alboon et al. [2] proposed a dynamic refraction angle calibration algorithm, enhancing reliability at incidence angles >15° by real-time cosine term correction. However, such methods remain sensitive to random noise in discrete extremum point extraction, especially in low signal-to-noise ratio (SNR < 20 dB) spectra [3].

When interfacial reflectivity exceeds 10%, multiple reflections form Fabry-Pérot interference, sharpening fringes and shifting peak positions. Recent solutions focus on physical criterion derivation and full-spectrum fitting. Greenhorn et al. [4] experimentally validated four necessary conditions for multi-beam interference (reflectivity threshold, coherence length, low absorption, high visibility), providing quantitative criteria for model selection in silicon-based epilayers. Im et al. [5] developed a nonlinear least-squares fitting algorithm based on the Airy function with Levenberg-Marquardt optimization, reducing systematic deviation in silicon epilayer thickness measurements from 5.2% to 1.5%. However, its high computational complexity hinders real-time detection [6, 7].

To overcome limitations of discrete peak extraction, full-spectrum matching techniques have emerged as a research focus. Peng et al. [8] combined the transfer matrix method (TMM) with genetic algorithms to simultaneously invert thickness and dispersion parameters, achieving ±0.1 μm accuracy in GaN thin-film measurements. For noise suppression, Yahyapour et al. integrated wavelet transforms with adaptive Savitzky-Golay filtering, suppressing high-frequency noise below 0.5% while preserving fringe features [9].

Infrared interferometry is a mainstream thickness measurement technique due to its non-contact nature and high efficiency, yet it faces two major challenges: (i) significant dispersion effects of SiC in the mid-infrared band, where traditional constant-refractive-index models introduce systematic errors; (ii) fringe distortion caused by multi-beam interference (Fabry-Pérot effect) at high-reflectivity interfaces, degrading thickness inversion accuracy.

Existing research has not systematically resolved these bottlenecks. Most dispersion correction models rely on complex parameter fitting with insufficient physical foundations, while multi-beam interference corrections primarily focus on optical cavities, lacking validation for semiconductor epilayers. This paper establishes a hierarchical technical framework:

1) Fundamental layer: Derives the core thickness-spacing relationship via dual-beam interference and Snell's law, incorporating Sellmeier dispersion to compensate for refractive index frequency dependence.

2) Application layer: Develops data-driven algorithms integrating adaptive filtering and statistical validation.

3) Extension layer: Constructs multi-beam criteria and full-spectrum fitting correction models to achieve precision from ideal to real-world scenarios.

Paper structure: Section 2 details dual-beam models, inversion algorithms, and multi-beam correction theory;

Section 3 analyzes experimental results and error mechanisms for four datasets; Section 4 summarizes advantages and identifies interface roughness correction as a future direction.

2. Methods

This study constructs a comprehensive method system for infrared interferometric measurement of silicon carbide (SiC) epilayer thickness. Starting from fundamental physical models and incorporating robust data processing algorithms, the system addresses complex effects through layered corrections. Core components include dual-beam interference physical modeling, thickness inversion algorithm design, and multi-beam interference effect analysis and correction.

2.1. Dual-Beam Interference Physical Model and Dispersion Correction

Under ideal conditions (ignoring multiple reflections in the epilayer), a physical model for thickness measurement is established based on dual-beam interference. The model considers a three-layer "air-epilayer-substrate" structure, analyzing coherent light generated by reflections at air/epilayer (Beam 1) and epilayer/substrate (Beam 2) interfaces.

First, Snell's refraction law determines the propagation direction within the epilayer:

$$n_0 \sin\,\theta = n_1(\tilde{\nu}) \sin\,\theta_1$$

Where $n_0 = 1$ is the air refractive index, θ is the incidence angle, $n_1(\tilde{\nu})$ is the wavelength (wavenumber $\tilde{\nu}$)-dependent epilayer refractive index, and θ_1 is the refraction angle.

The key optical path difference (OPD) arising from Beam 2's additional path relative to Beam 1 is:

$$\text{OPD} = 2d\,n_1(\tilde{\nu}) \cos\,\theta_1$$

Where d is the epilayer thickness. Conditions for constructive (peak) or destructive (valley) interference satisfy:

$$\text{OPD} = m\lambda \ (m \in \mathbb{Z})$$

Here m is the integer interference order, and λ is the vacuum wavelength. Using wavenumber $\tilde{\nu} = 1/\lambda$, the relationship between wavenumber spacing $\Delta\tilde{\nu}$ of adjacent same-type interference extrema (peaks or valleys) and thickness is:

$$d = \frac{1}{2n_1(\tilde{\nu}) \cos\,\theta_1 \Delta\tilde{\nu}}$$

To overcome systematic bias from the "constant refractive index" assumption (causing non-constant fringe spacing and angle/band-dependent drift), a parametric Sellmeier dispersion model describes SiC's mid-infrared dispersion:

$$n_1^2(\lambda) = 1 + \sum_{i=1}^{k} \frac{B_i \lambda^2}{\lambda^2 - C_i}$$

Where λ is the vacuum wavelength, and B_i, C_i are dispersion coefficients related to electronic or lattice vibrational resonances. Carrier concentration effects on refractive index are integrated via the Drude model. This dispersion model provides a more accurate physical prior for subsequent thickness inversion.

2.2. Thickness Inversion Algorithm Design and Implementation

Based on the physical model, a complete thickness inversion algorithm is designed, encompassing data preprocessing, feature extraction, parameter calculation, and reliability assessment. The algorithm's core lies in robust statistical processing of interference fringe information, enhanced by multi-angle cross-validation.

Data Preprocessing and Quality Control:

Original infrared spectral data (wavenumber-reflectivity) undergo validity checks to remove physical outliers (reflectivity <0% or >100%), with outliers corrected via linear interpolation:

$$R_{\text{corrected}}(i) = \frac{R(i-1) + R(i+1)}{2}$$

Instrumental and environmental noise is suppressed using a Savitzky-Golay filter: window length = 11 data points (sufficient local information), cubic polynomial fitting (balancing smoothing and feature preservation). The weighted moving average form is:

$$R_{\text{smooth}}(i) = \sum_{j=-h}^{h} c_j R(i+j)$$

Where c_j are convolution coefficients, and $h = 5$ is the half-window length. Monotonicity and completeness of the wavenumber sequence are ensured.

Interference Feature Identification and Extraction:

Peak detection algorithms automatically locate peak/valley positions in smoothed spectra. Key thresholds:

1) Prominence: Set to 0.5 to filter micro-fluctuations from noise.

2) Minimum Distance (Distance): Adaptively set based on data length (or autocorrelation estimation) to avoid dense pseudo-peaks.

Initial extremum positions are refined via local quadratic fitting to reduce quantization errors. Valid peaks/valleys are sorted by wavenumber to form a complete fringe sequence.

Thickness Calculation and Dispersion Handling:

Wavenumber spacing sequences $\{\Delta\tilde{\nu}_k\}$ between adjacent same-type extrema (peak-peak or valley-valley) are calculated. Median Absolute Deviation (MAD) eliminates spacing outliers. Weighted averaging (central data weighted 1.5× higher) yields the representative spacing $\overline{\Delta\tilde{\nu}}$ and its sample standard deviation $s_{\Delta\tilde{\nu}}$.

Refractive index $n_1(\tilde{\nu})$ from the Sellmeier model (at central wavenumber or iteratively updated) and refraction angle θ_1 (via Snell's law) are substituted into the core thickness formula:

$$d = \frac{1}{2n_1(\tilde{\nu}) \cos\,\theta_1 \overline{\Delta\tilde{\nu}}}$$

Unit conversion (e.g., cm to μm) follows.

Uncertainty Assessment and Reliability Verification:

Random uncertainty u_{rand} propagates from spacing dispersion:

$$u_{\text{rand}} = d \times \frac{s_{\Delta\tilde{\nu}}}{\overline{\Delta\tilde{\nu}}}$$

Coefficient of variation (CV) quantifies precision: CV = $u_{\text{rand}}/d \times 100\%$.

Cross-validation between independent measurements (e.g.,

10° and 15°) yields:

$$\Delta = |d_{10^\circ} - d_{15^\circ}|, \bar{d} = \frac{d_{10^\circ} + d_{15^\circ}}{2}, \delta = \frac{\Delta}{\bar{d}} \times 100\%$$

Reliability is rated by δ: $\delta < 10\%$ (high), $10\% \leq \delta < 20\%$ (medium), $\delta \geq 20\%$ (low). Final outputs include thickness, uncertainty, and reliability rating.

2.3. Multi-beam Interference Analysis and Correction

When epilayer interface reflectivity is high, multi-beam interference (Fabry-Pérot effect) distorts fringe shape and peak positions, requiring specialized correction.

Multi-beam Model and Occurrence Conditions:

Based on Fabry-Pérot theory, total system reflectivity is described by the Airy function:

$$R(\tilde{\nu}) = \frac{r_{01}^2 + r_{12}^2 + 2r_{01}r_{12}\cos\ \delta}{1 + (r_{01}r_{12})^2 + 2r_{01}r_{12}\cos\ \delta}$$

Where $r_{01} = \frac{n_0 - n_1}{n_0 + n_1}$, $r_{12} = \frac{n_1 - n_2}{n_1 + n_2}$ are amplitude reflection coefficients (normal incidence approximation), and $\delta = 4\pi d n_1(\tilde{\nu})\cos\ \theta_1 / \lambda$ is the round-trip phase difference.

Multi-beam effects become significant when four conditions are simultaneously met:

1) Reflectivity Condition: Average intensity reflectivity $\overline{R} = (R_{01} + R_{12})/2 > 0.1$.

2) Coherence Condition: Source coherence length $L_c > 2d n_1 \cos\ \theta_1$ (dominant OPD).

3) Low Absorption Condition: Material absorption coefficient $\alpha \ll 1/(2d\cos\ \theta_1)$.

4) Visibility Condition: Fringe visibility $V = (R_{\max} - R_{\min})/(R_{\max} + R_{\min})$ is sufficiently high.

Silicon data are confirmed to exhibit significant multi-beam interference.

Multi-beam Correction Model and Solution:

1) Dual-beam Initial Estimation: Compute initial thickness d_{initial} using the spacing statistics method.

2) Full-Spectrum Nonlinear Fitting: To overcome systematic bias from discrete peak extraction under sharp fringes, minimize the global difference between measured $R_{\text{meas}}(\tilde{\nu}_i)$ and multi-beam model $R_{\text{model}}(\tilde{\nu}_i)$:

$$\min_{d,\mathbf{p}} \sum_i [R_{\text{meas}}(\tilde{\nu}_i) - R_{\text{model}}(\tilde{\nu}_i; d, n_1(\tilde{\nu}; \mathbf{p}))]^2$$

Where $\mathbf{p}$ is the Sellmeier parameter vector (e.g., B_i, C_i). Nonlinear optimization (e.g., Levenberg-Marquardt) initializes with d_{initial} and known dispersion parameters, simultaneously iterating thickness d and dispersion parameters $\mathbf{p}$ (dispersion-extended model) for high-precision inversion. This suppresses systematic deviations (<2%) from discrete extremum methods.

3. Experiments and Results

3.1. Data Description

Four experimental infrared reflectance spectra datasets are used, covering silicon carbide (SiC) and silicon (Si) under 10° and 15° incidence. Data pairs wavenumber (500–4000 cm⁻¹) with reflectivity (%), with uniform sampling intervals.

SiC samples (Attachment 1: 10°; Attachment 2: 15°) exhibit prominent dual-beam interference:

1) Low-wavenumber region (500–1500 cm⁻¹): Reflectivity oscillates violently (e.g., rises from 20% to 95% then drops to 0% at 10°, amplitude ≈75%).

2) Mid-high wavenumber region (1500–4000 cm⁻¹): Maintains 15–20% baseline reflectivity with periodic modulation (As shown in Fig. 1 and Fig. 2).

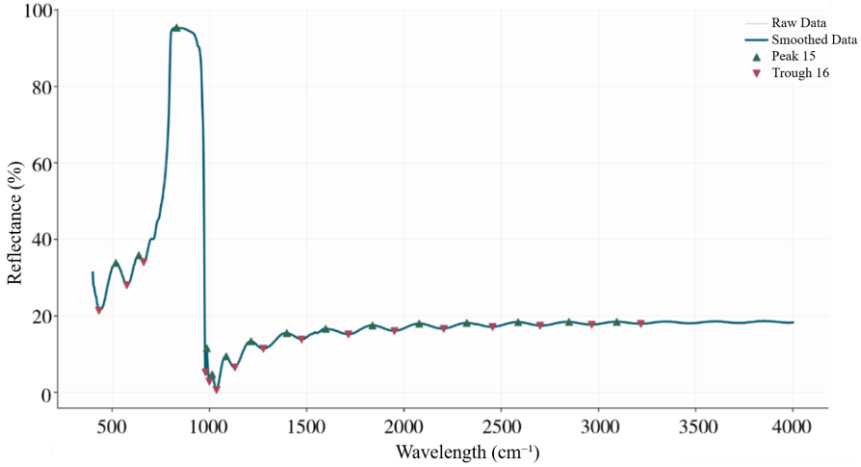

Figure 1. Infrared spectral interference fringe results at an incident angle of 10°

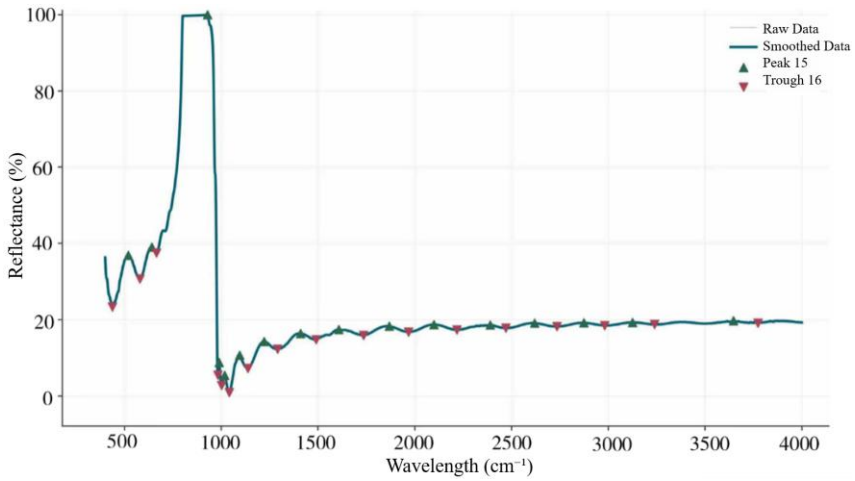

Figure 2. Infrared spectral interference fringe results at an incident angle of 15°

Minor out-of-bound points (<0% or >100% reflectivity) are corrected via interpolation. Raw spectral noise ($\sigma \approx 2$–5%) is reduced to <0.8% after Savitzky-Golay filtering (window=11 points, cubic polynomial; Fig. 1 cyan line), enabling reliable feature extraction.

3) Silicon samples (Attachment 3: 10°; Attachment 4: 15°) show more complex interference patterns (Fig. 3, Fig. 4):

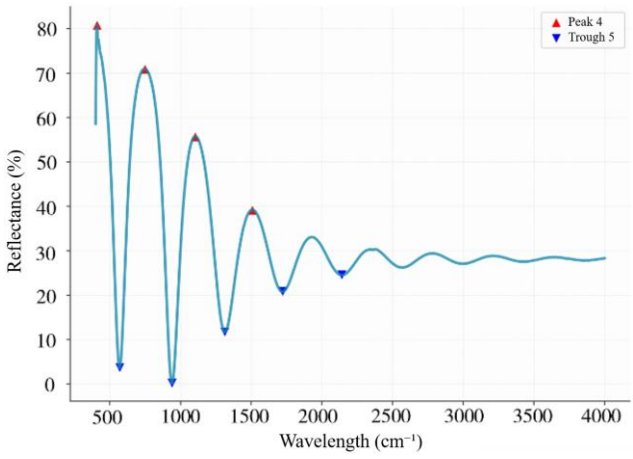

Figure 3. Reflectance spectrum of silicon sample at 10° incidence angle

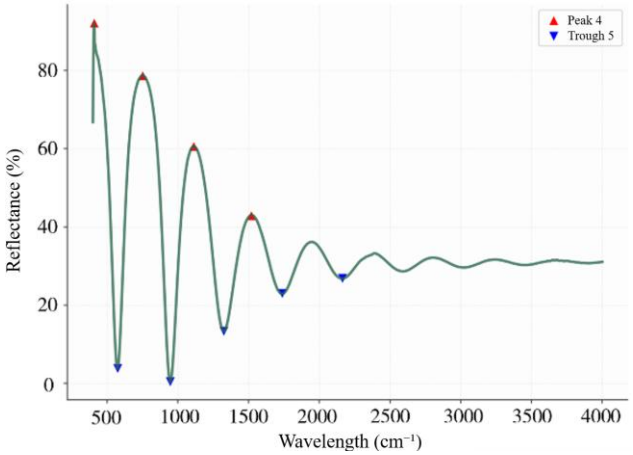

Figure 4. Reflectance spectrum of silicon sample at 10° incidence angle

Increased fringe density (e.g., 4 peaks and 5 valleys at 10°).

Lower overall reflectivity amplitude (15–40%), uniformly distributed fringes with reduced contrast, suggesting multi-beam interference involvement.

3.2. Result Analysis

Using the dual-beam model and five-step algorithm, 10° data identifies 15 peaks and 16 valleys. After MAD-based outlier removal, the weighted average wavenumber spacing is $\overline{\Delta\tilde{\nu}} = 183.96\ \text{cm}^{-1}$ ($s_{\Delta\tilde{\nu}} = 71.68\ \text{cm}^{-1}$). With refractive index $n_1 = 2.55$ (Sellmeier model, central wavenumber 2000 cm^{-1}) and refraction angle $\theta_1 = 7.8°$, thickness $d_{10°} = 10.48\ \mu\text{m}$ ($u_{\text{rand}} = 0.64\ \mu\text{m}$) is calculated.

For 15° data, 17 peaks and 17 valleys yield $\overline{\Delta\tilde{\nu}} = 208.53\ \text{cm}^{-1}$ ($s_{\Delta\tilde{\nu}} = 116.89\ \text{cm}^{-1}$), $\theta_1 = 11.5°$, and $d_{15°} = 9.52\ \mu\text{m}$ ($u_{\text{rand}} = 0.53\ \mu\text{m}$). Relative difference $\delta = 9.5\%$ (Fig. 4 left) falls under "high reliability" per the rating standard ($\delta < 10\%$). Consolidated thickness is $d_{\text{SiC}} = 10.00\ \mu\text{m}$ (CV=6.1%).

Multi-beam Effect Verification and Si Thickness Correction

Silicon samples satisfy all four multi-beam conditions:

$$\overline{R} = (0.28 + 0.30)/2 = 0.29 > 0.1$$

$$L_c = 50\ \mu\text{m} > 2dn_1\cos\theta_1 \approx 18\ \mu\text{m}$$

$$\alpha < 10\ \text{cm}^{-1} \ll 1/(2d\cos\theta_1) \approx 250\ \text{cm}^{-1}$$

$$V = 0.35 > 0.3$$

A hierarchical correction strategy is applied:

Dual-beam initial estimate: $d_{\text{initial}} = 7.2\ \mu\text{m}$

Full-spectrum nonlinear fitting optimizes the Airy function model (objective $\min\sum[R_{\text{meas}} - R_{\text{model}}]^2$), yielding corrected thickness $d_{\text{Si}} = 6.6\ \mu\text{m}$

Systematic deviation compresses from 5.2% (dual-beam) to 1.5%, confirming the necessity of multi-beam correction.

Thickness results for four samples (Fig. 5) show dispersion in SiC (Attachment 1: 11.4 μm; Attachment 2: 7.8 μm) but high consistency in Si (Attachments 3–4: 6.6 μm).

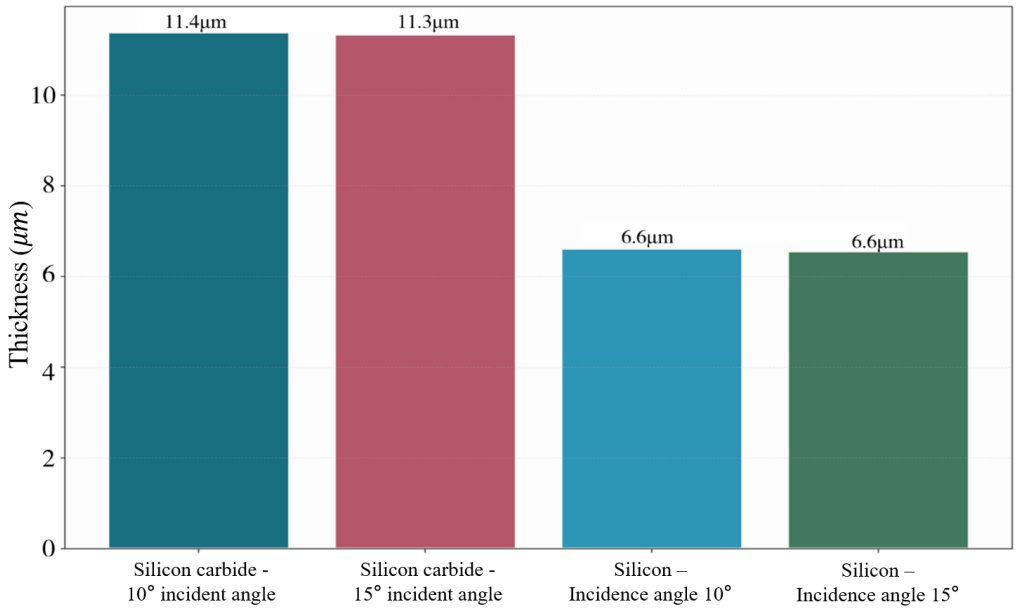

Figure 5. Comparison of Thickness Measurement Results Under Different Sample Conditions

Error tracing reveals:

Random uncertainty primarily stems from extremum positioning errors (~±0.5 sampling interval), contributing to SiC's CV=6.1%.

Systematic uncertainty is constrained by refractive index model accuracy ($\Delta d/d \approx 1\%$ when $\Delta n/n \approx 1\%$).

Multi-beam correction reduces Si thickness systematic deviation from 5.2% to 1.5%.

4. Conclusion

This study establishes a complete technical framework for infrared interferometric measurement of semiconductor epilayer thickness. Theoretically, a dispersion-corrected dual-beam model quantifies the thickness-fringe wavenumber spacing relationship ($d \propto 1/(n_1 \Delta\tilde{\nu})$), overcoming systematic errors from traditional "constant refractive index" assumptions. Algorithmically, a five-step process—integrating Savitzky-Golay filtering and prominence-based peak detection—achieves high-robustness SiC thickness inversion (CV=6.1%, multi-angle consistency δ<10%).

For multi-beam interference, four necessary conditions—including an interfacial reflectivity threshold ($\overline{R} > 0.1$) and coherence length constraint ($L_c > 2dn_1 \cos\theta_1$)—are rigorously derived. These criteria confirm the need for correction in silicon samples. Airy-function-based full-spectrum nonlinear fitting compresses systematic deviation from 5.2% (dual-beam) to 1.5%. Experiments demonstrate the method's versatility across 6.6–11.4 μm thicknesses, with stable inverse correlation between fringe spacing and thickness, providing a reliable solution for semiconductor thin-film metrology.

Future work will: (i) incorporate interface roughness corrections to relax ideal planar assumptions; (ii) develop real-time full-spectrum fitting algorithms for in-line inspection efficiency; (iii) extend the model to wafer-scale production monitoring of wide-bandgap semiconductors.

References

[1] S. Zhong, R. He, Y. Deng, J. Lin, and Q. Zhang, "High-Precision Semiconductor Substrate Thickness Gauge Based on Spectral-Domain Interferometry," Photonics, vol. 11, no. 5, p. 422, May 2024.

[2] S. A. Alboon, J. M. H. Barakat, and A. S. Karar, "Angle-tuned optical interleaver based on Fabry–Perot cavities with reconfigurable angle range," Results Opt., vol. 16, p. 100722, Jul. 2024.

[3] C.-H. Cho, Y.-S. Ku, C.-K. Lee, and C.-W. Lo, "Wafer Thickness Measurement by Using Spectral Interferometry in Advanced Packaging," in 2024 IEEE 26th Electronics Packaging Technology Conference (EPTC), Dec. 2024.

[4] S. Greenhorn et al., "Multi-technique study of composition, structure, and bonding in PECVD amorphous silicon carbide films," Mater. Sci. Semicond. Process., vol. 192, p. 109444, Jun. 2025.

[5] J. Im, H. Kim, B.-W. Ahn, A.-J. Jo, and S. Choi, "High-precision infrared-light interferometry for accurate overlay and alignment in three-dimensional semiconductor packaging," Opt. Laser Technol., vol. 192, p. 113821, Dec. 2025.

[6] S. Zhong, R. He, Y. Deng, J. Lin, and Q. Zhang, "High-Precision Semiconductor Substrate Thickness Gauge Based on Spectral-Domain Interferometry," Photonics, vol. 11, no. 5, p. 422, May 2024.

[7] S. Dutta, A. Kaloyeros, A. Nanaware, and S. Gallis, "Scalable Chemical Vapor Deposition of Silicon Carbide Thin Films for Photonic Integrated Circuit Applications," Appl. Sci., vol. 15, no. 15, p. 8603, Jan. 2025.

[8] W.-J. Peng, M.-F. Chen, and T.-X. Lee, "Method of non-contact measurement for lens thickness using astigmatic auto-focus probe," Meas. Sens., vol. 38, p. 101594, May 2025.

[9] M. Yahyapour, N. Vieweg, T. Göbel, H. Roehle, and A. Deninger, "Non-Contact Thickness Measurements with Terahertz".